Supplementary of

Contrasting large river basins are characterized by high fractions of young water and show differences in water-age dynamics across flow conditions and seasons

Karl Knabel et al.

Correspondence to: Karl Knaebel (karl.knaebel@boku.ac.at)

Tab. S1 Equations governing the individual storage reservoirs in the hydrological model: interception, snow, unsaturated-zone, fast-flow, and slow-flow reservoirs (e.g., Gao et al., 2017; Gao et al., 2014; Hrachowitz et al., 2013; Hrachowitz et al., 2021; Prenner et al., 2018).

Reservoirs	Water balance	Constitutive equations
Interception reservoir	$\frac{dS_i}{dt} = P_{rain} - E_i - P_r$	$P_{rain} = P, if\ T > T_t$ $E_i = \min(E_p, S_i/dt)$ $P_n = \max((S_i - S_{imax})/dt, 0)$
Snow reservoir	$\frac{dS_{snow}}{dt} = P_{snow} - M_{snow}$	$P_{snow} = P, if\ T \leq T_t$ $M_{snow} = \min(C_{melt}(T - T_t), S_{snow}/dt), if\ T > T_t$
Unsaturated reservoir	$\frac{dS_u}{dt} = P_e - E_a - R_u - R_{perc}$	$P_e = P_n + M_{snow}$ $\rho = S_u/S_{max}$ $E_a = (E_p - E_i) * \min(\rho/C_a, 1)$ $C_r = 1 - (1-\rho)^\gamma$ $R_u = (1 - C_r) P_e$ $R_{perc} = \min(c_{pmax}\ \rho, S_u/dt)$ $R_{pref} = (1 - D) R_u$
Fast reservoir	$\frac{dS_f}{dt} = R_f - Q_f$	$R_f = D\ R_u$ $Q_f = K_f\ S_f$
Slow reservoir	$\frac{dS_s}{dt} = R_{perc} + R_{pref} - Q_s$	$Q_s = K_s\ S_s$

Pr = real rainfall after interception per elevation zone

Pe = P effective precipitation i.e., Snow + Pr

Tab. S2 Constitutive equations governing the river-routing routine.

	Equations
None routed discharge	$Q_g = Q_s + Q_f$
Routing kernel length	If Tp > 0; else no routing: $L = 2\,T_p + 1$
Triangular routing kernel and weights	$K = \{k_i\}_{i=0}^{L-1}$ $k_i = \frac{T_p - \lvert i - T_p \rvert}{T_p^2}$ $\sum_{i=0}^{L-1} k_i = 1$
River routing	$Q_m[k] = \sum_{i+j=k} Q_g[i]\,K[j]\; for\; i \in [0, N-1], j[0, L-1]$
Tracer mass routing	$Tracer_{mass\ routed}[k] = \sum_{i+j=k} \left(Q_g[i]\,K[j]\right) Tracer_{con}[i]\; for\; i \in [0, N-1], j[0, L-1]$
Routed tracer concentration	$Tracer_{con\ routed}[k] = \frac{Tracer_{mass\ routed}[k]}{Q_m[k]}$
Symbols and explanations	i = input day, j = travel time (i.e., the delay days from the kernel), k = j + i = arrival day (i.e., the day the signal appears at the outlet), $Q_g[i]$ = the input flow volume on day K[j] = the fractional weight of the kernel for delay j $Tracer_{con}[i]$ = tracer concentration of Qg[i] on day i

Tab. S3 Elevation zones, elevation ranges (m), and fractional basin areas (Frac.) for the six river basins. Zones are ordered from lower to higher elevations, with up to six zones used depending on the basin.

Zones	Elbe	Elbe	Ems	Ems	Main	Main	Moselle	Moselle	Neckar	Neckar	Oder	Oder
	Range	Frac.	Range	Frac.	Range	Frac.	Range	Frac.	Range	Frac.	Range	Frac.
1	200 m	0.465	200 m	1	300 m	0.325	300 m	0.712	300 m	0.383	200 m	0.759
2	400 m	0.242			500 m	0.609	500 m	0.237	500 m	0.436	400 m	0.175
3	600 m	0.215			700 m	0.063	700 m	0.036	700 m	0.168	600 m	0.045
4	800 m	0.065			> 700 m	0.003	> 900m	0.015	> 700 m	0.013	800 m	0.017
5	1000 m	0.011									1000 m	0.004
6	> 1000 m	0.002									> 1000 m	0.001

Tab. S4 Time periods used for model calibration and testing together with the preceding warm-up (spin-up) periods.

Basin	Warm-up testing	Testing	Warm-up calibration	Calibration
Elbe	1950 – 1960	1960 – 1980	1980 – 2001	2001 – 2020
Ems	1964 – 1970	1970 – 1980	1980 – 2001	2001 – 2020
Main	1963 – 1970	1970 – 1980	1980 – 2001	2001 – 2020
Moselle	1950 – 1960	1960 – 1980	1980 – 2001	2001 – 2020
Neckar	1950 – 1960	1960 – 1980	1980 – 2001	2001 – 2020
Oder	1950 – 1960	1960 – 1980	1980 – 2001	2001 – 2020

Tab. S5 Model parameter ranges for the top 20% of Pareto-optimal parameter sets (i.e., those with the lowest D_E values) among the six river basins, together with the initial pre-calibration parameter ranges.

Parameter	initial range	Elbe	Ems	Main	Moselle	Neckar	Oder
T_t (°C)	-2.5 – 2.5	-1.76 – 0.64	-2.49 – 1.99	-1.73 – 1.28	-2.16 – 0.84	-2.31 – 1.63	-2.11 – 0.45
γ (–)	0.1 – 5.0	0.14 – 0.61	0.31 – 1.61	0.23 – 1.70	0.19 – 1.35	0.46 – 2.36	0.21 – 1.07
C_a (–)	0.1 – 0.7	0.31 – 0.70	0.13 – 0.44	0.15 – 0.52	0.29 – 0.70	0.14 – 0.46	0.25 – 0.69
C_{melt} (mm °C^{-1} d^{-1})	1.0 – 5.0	1.03 – 4.97	1.00 – 5.00	1.05 – 5.00	1.12 – 4.98	1.01 – 5.00	1.16 – 4.99
C_{pmax} (mm d^{-1})	0.1 - 4.0	0.32 – 1.01	0.56 – 2.52	0.10 – 1.44	0.20 – 1.01	0.55 – 3.53	0.31 – 1.19
D (–)	0.01 – 1.0	0.54 – 0.99	0.54 – 0.95	0.38 – 0.82	0.51 – 0.94	0.44 – 0.89	0.51 – 0.99
K_f (d^{-1})	0.2 – 5.0	0.20 – 4.97	0.23 – 5.00	0.22 – 4.97	0.21 – 4.99	0.27 – 4.98	0.20 – 4.99
K_s (d^{-1})	0.002 – 0.2	0.05 – 0.20	0.04 – 0.20	0.01 – 0.11	0.03 – 0.19	0.02 – 0.19	0.03 – 0.18
Simax (mm)	0.1 – 5.0	0.11 – 1.27	0.10 – 1.31	0.10 – 1.25	0.11 – 3.00	0.10 – 1.71	0.10 – 1.64
Ssp (mm)	3000 – 20000	12965 – 19995	14243 – 19995	7992 – 19979	10582 – 19888	12711 – 19988	12370 – 19981
Sumax (mm)	100 – 500	172 – 436	194 – 499	182 – 496	140 – 303	207 – 499	224 – 498
Tp (d)	0 – 12	9 – 12	2 – 5	1 – 5	1 – 4	1 – 2	10 – 12

Tab. S6 Snow cover equations as presented in Parajka and Blöschl, 2008.

Snow covered area (SCA)	$SCA = \frac{S}{S+L}$ where S = number of pixel snow, L = number of pixel land
Snow cover model overestimation error (S_E^O)	$S_E^O = \frac{1}{m}\sum m_o \wedge (SWE > 0\ mm) \wedge (SCA \leq 25\%)$ where m_O = number of days when model simulates snow cover i.e., SWE > 0mm but MODIS snow cover indicates no snow is present i.e., SCA ≤ 25%, m = number of day where MODIS data is available i.e., cloud cover ≤ 60%
Snow cover model underestimation error (S_E^U)	$S_E^U = \frac{1}{m}\sum m_U \wedge (SWE = 0\ mm) \wedge (SCA > 25\%)$ where m_U = number of days when the model does not simulate snow cover i.e., SWE = 0 mm but MODIS snow cover indicates no snow is present i.e., SCA > 25%, m = number of day where MODIS data is available i.e., cloud cover ≤ 60%
Combined snow cover error (S_E)	$S_E = S_E^O + S_E^U$

Fig. S1 Observed and modelled discharge, with uncertainty intervals based on the 95% range of all retained Pareto-optimal solutions, for the six basins during October 2001–December 2020.

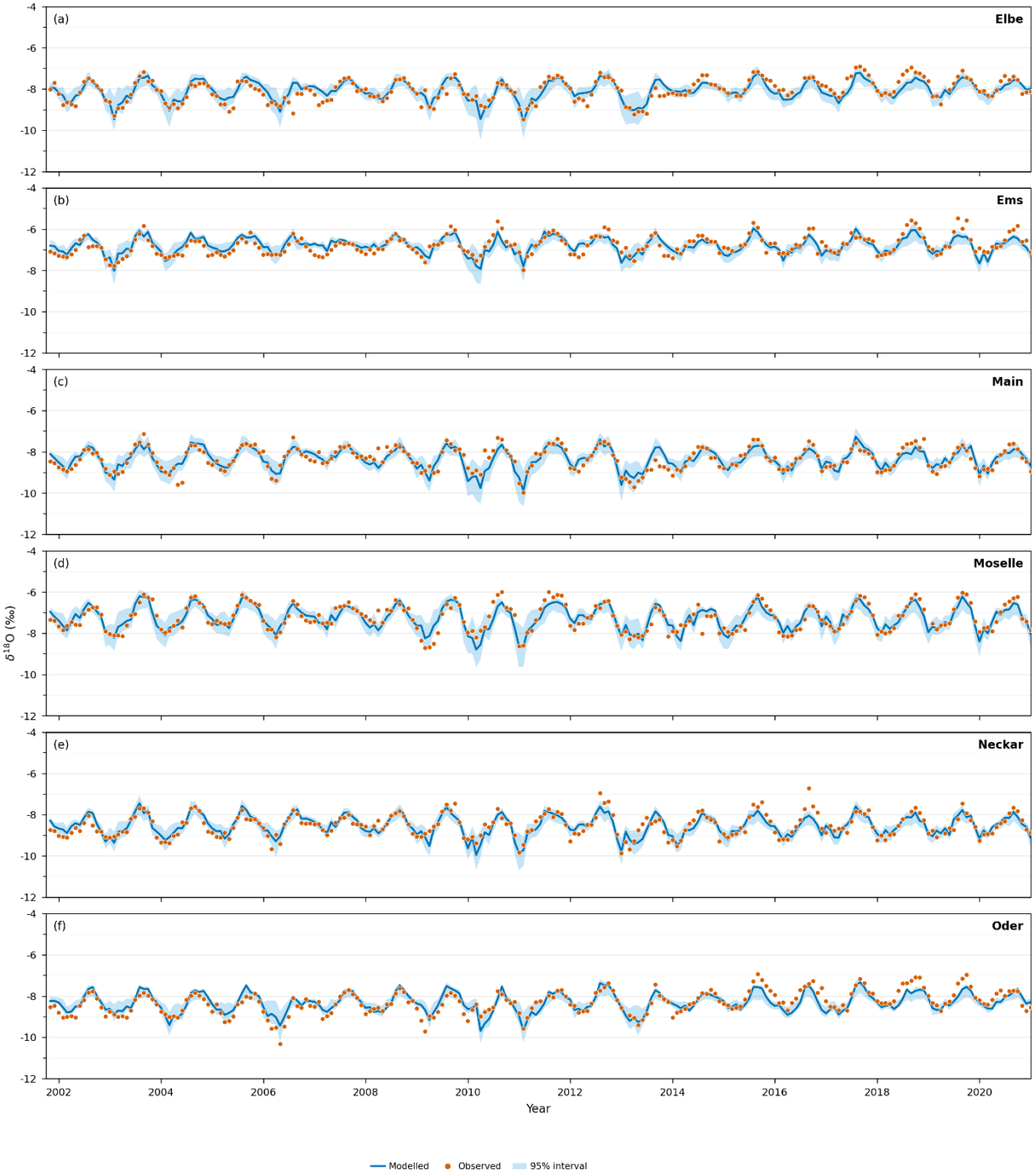

Fig. S2 Observed and modelled discharge, together with uncertainty intervals derived from the 95% range of all retained Pareto-optimal solutions, for the six basins during October 2001–December 2020.

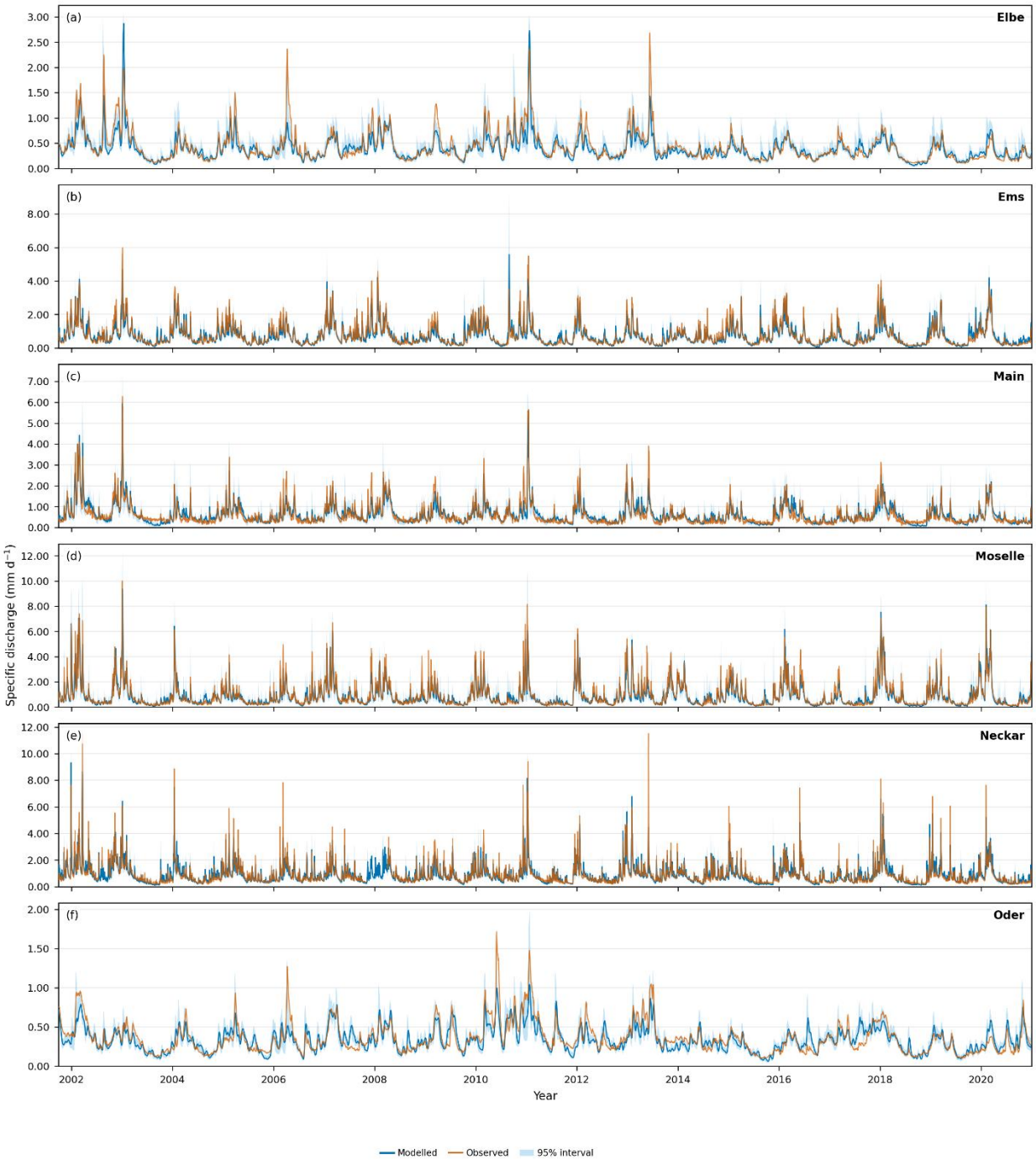

Fig. S3 Observed and modelled flow-duration curves, with uncertainty intervals based on the 95% range of all retained Pareto-optimal solutions, for the six basins during October 2001–December 2020.

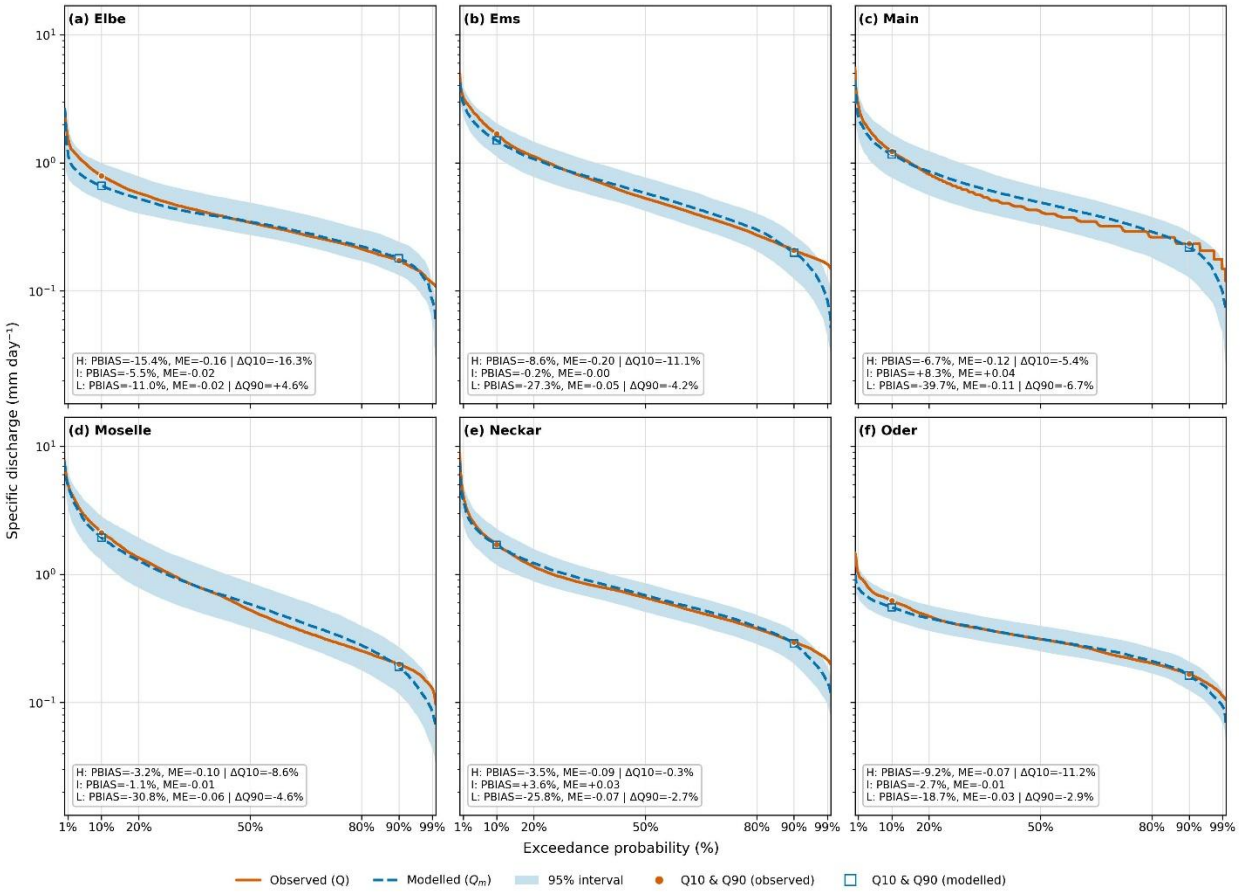

Fig. S4 Observed and modelled seasonal runoff coefficients, with uncertainty intervals based on the 95% range of all retained Pareto-optimal solutions for the six basins during October 2001–December 2020.

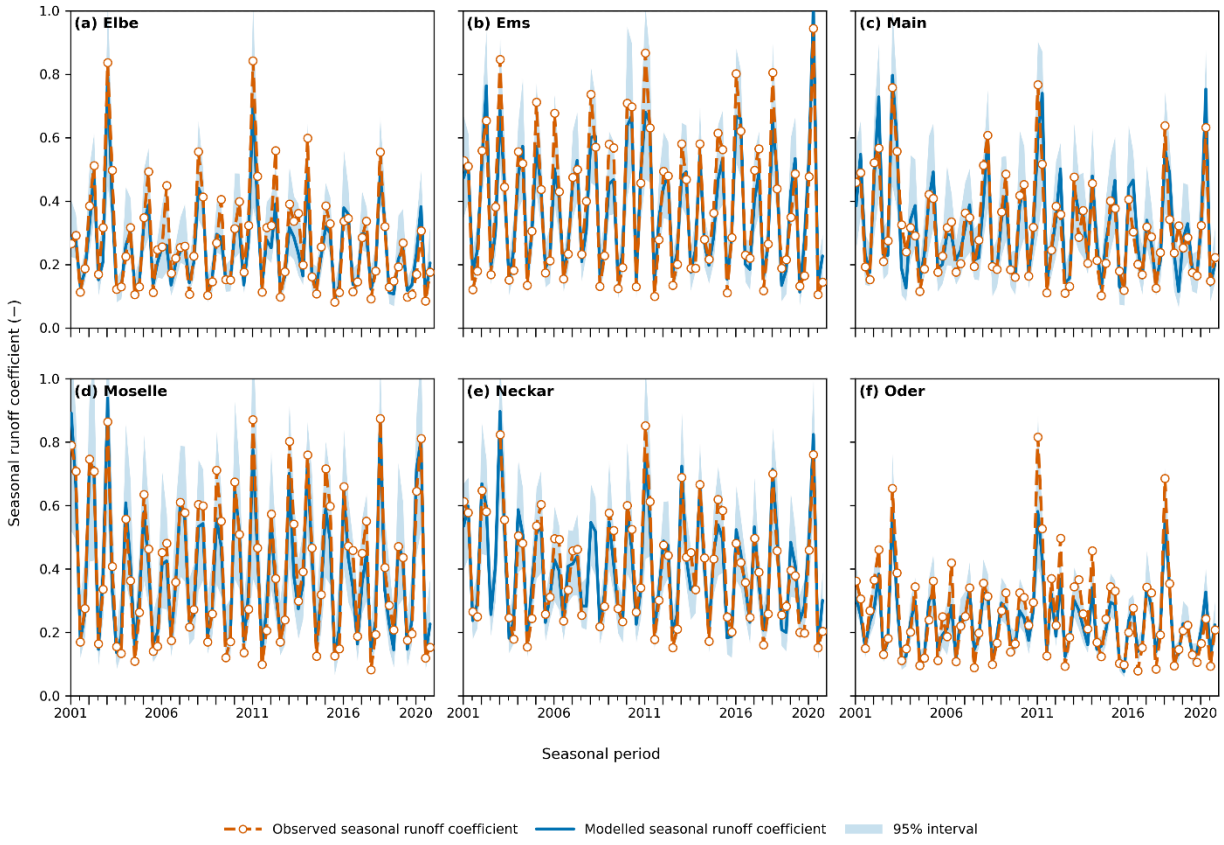

Tab. S7 Snow-cover errors, including total error (%), overestimation error (%), and underestimation error (%), for all six studied basins based on the best-performing parameter set with the lowest D_E.

Snow cover errors	Elbe	Ems	Main	Moselle	Neckar	Oder
Total snow cover error (%)	8.34	9.1	8.84	6.90	8.55	9.05
Overestimation (%)	3.81	3.28	6.09	3.71	4.55	3.57
Underestimation (%)	4.52	5.83	2.75	3.20	4.00	5.47

Tab. S8 Modelled high-flow (Q_{m10}), median-flow (Q_{m50}), and low-flow (Q_{m90}) discharge thresholds.

Catchment	Q_{m90}	Q_{m50}	Q_{m10}
Elbe	0.17	0.34	0.66
Ems	0.19	0.58	1.49
Main	0.21	0.49	1.16
Mosel	0.18	0.58	1.94
Neckar	0.29	0.69	1.70
Oder	0.16	0.31	0.55

Fig. S5 Violin plots of the different water-age fractions under high-, intermediate-, and low-flow regimes for all six basins.

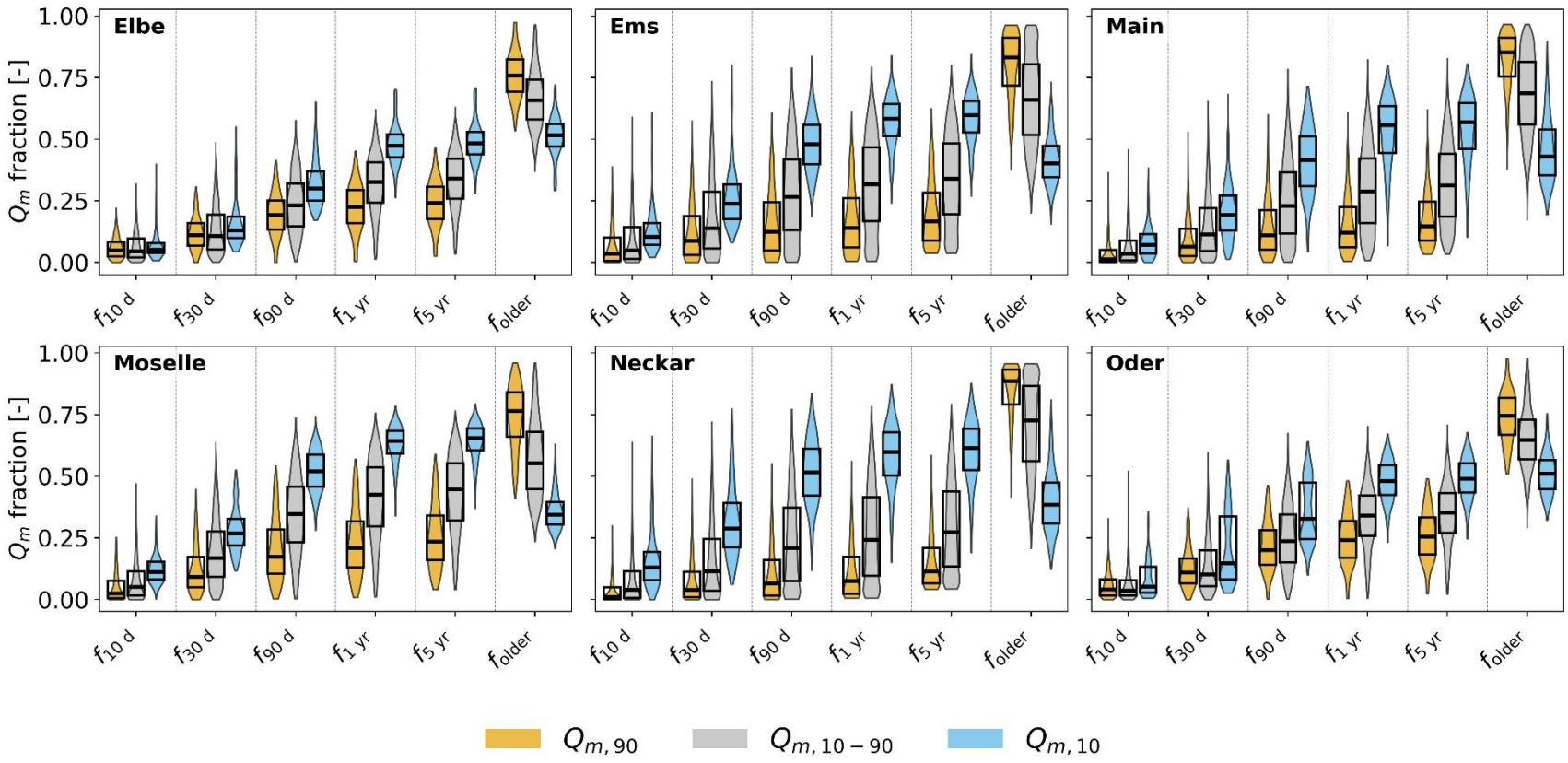

Fig S6 Exemplary summer (1) and winter (2) high-flow events for the Elbe (a), Ems (b), Main (c), Moselle (d), Neckar (e), and Oder (f) basins. The hydrographs are partitioned into normalized water-age fractions, ranging from 0 to 1 at each time step and shaded from light grey (younger water) to dark grey (older water). Modelled sdischarge Q_m is shown in color.

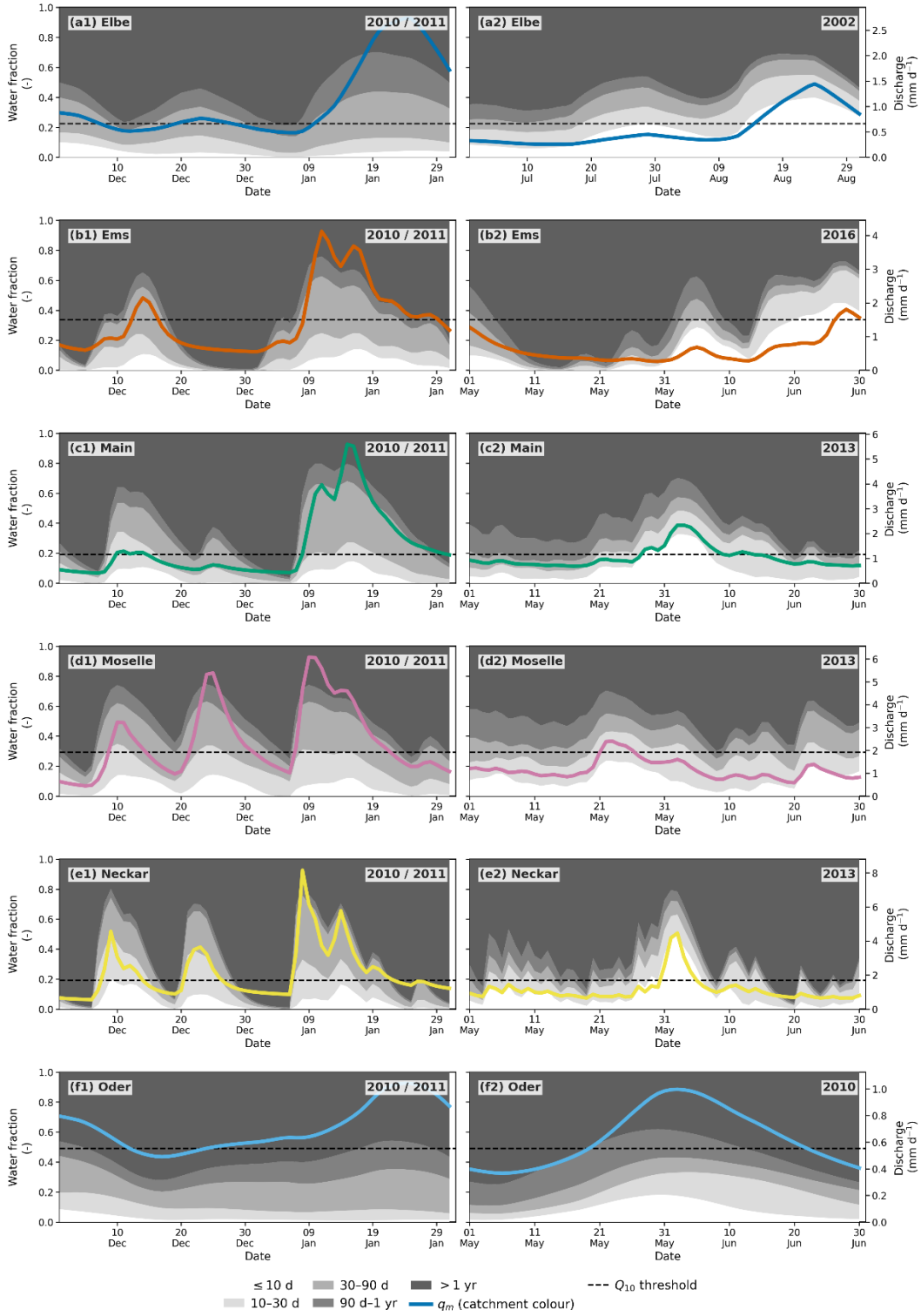

Fig S7 Spearman rank-correlation coefficient (r_s) matrices for the six basins. Asterisks (*) indicate statistically significant correlations i.e., $p < 0.05$.

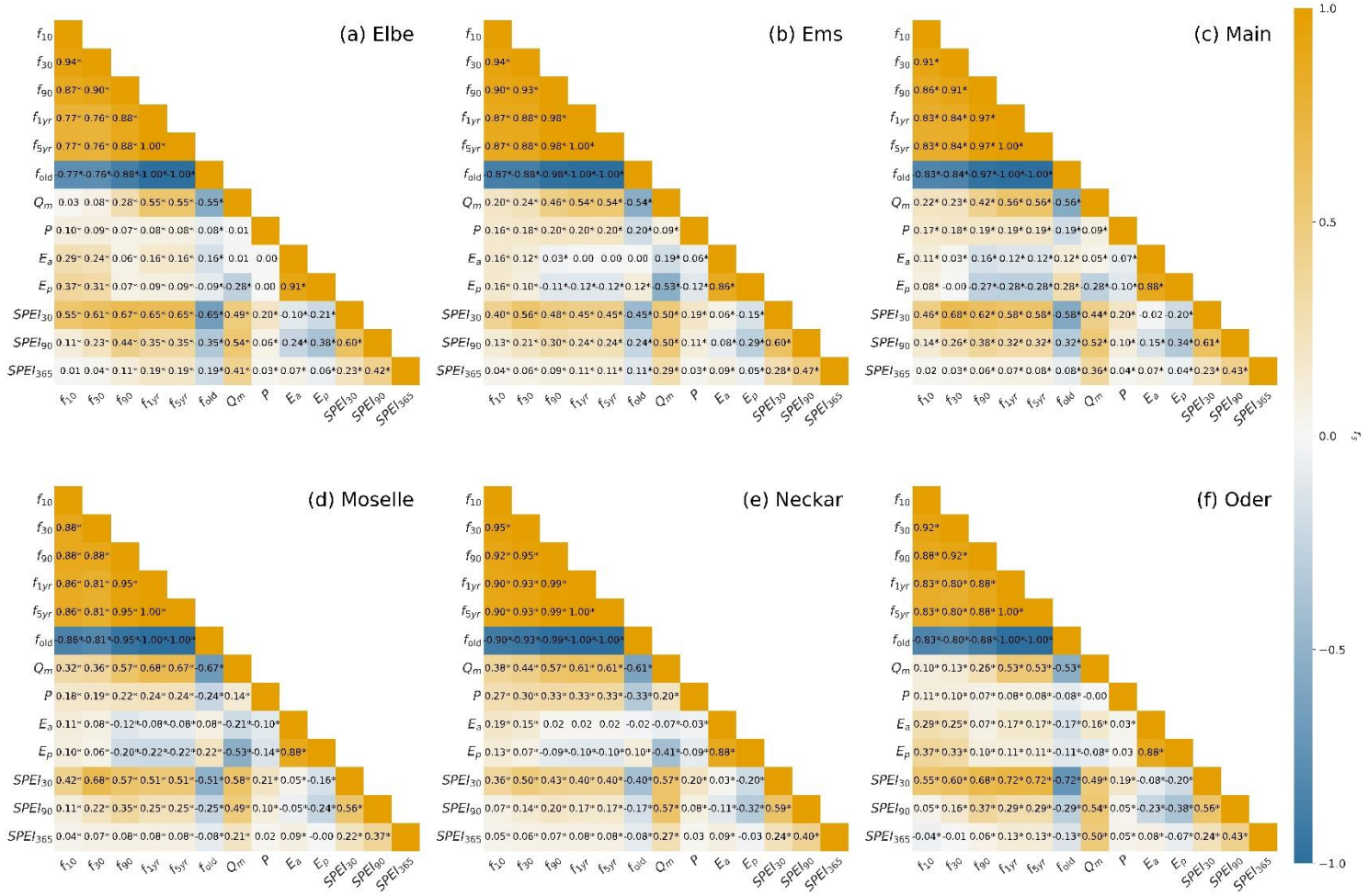

References

Gao, H., Ding, Y., Zhao, Q., Hrachowitz, M., and Savenije, H. H.: The importance of aspect for modelling the hydrological response in a glacier catchment in Central Asia, Hydrological Processes, 31, 2842–2859, doi:10.1002/hyp.11224, 2017.

Gao, H., Hrachowitz, M., Fenicia, F., Gharari, S., and Savenije, H. H. G.: Testing the realism of a topography-driven model (FLEX-Topo) in the nested catchments of the Upper Heihe, China, Hydrol. Earth Syst. Sci., 18, 1895–1915, doi:10.5194/hess-18-1895-2014, 2014.

Hrachowitz, M., Savenije, H., Bogaard, T. A., Tetzlaff, D., and Soulsby, C.: What can flux tracking teach us about water age distribution patterns and their temporal dynamics?, Hydrol. Earth Syst. Sci., 17, 533–564, doi:10.5194/hess-17-533-2013, 2013.

Hrachowitz, M., Stockinger, M., Coenders-Gerrits, M., van der Ent, R., Bogena, H., Lücke, A., and Stumpp, C.: Reduction of vegetation-accessible water storage capacity after deforestation affects catchment travel time distributions and increases young water fractions in a headwater catchment, Hydrol. Earth Syst. Sci., 25, 4887–4915, doi:10.5194/hess-25-4887-2021, 2021.

Parajka, J. and Blöschl, G.: The value of MODIS snow cover data in validating and calibrating conceptual hydrologic models, Journal of Hydrology, 358, 240–258, doi:10.1016/j.jhydrol.2008.06.006, 2008.

Prenner, D., Kaitna, R., Mostbauer, K., and Hrachowitz, M.: The Value of Using Multiple Hydrometeorological Variables to Predict Temporal Debris Flow Susceptibility in an Alpine Environment, Water Resour. Res., 54, 6822–6843, doi:10.1029/2018WR022985, 2018.